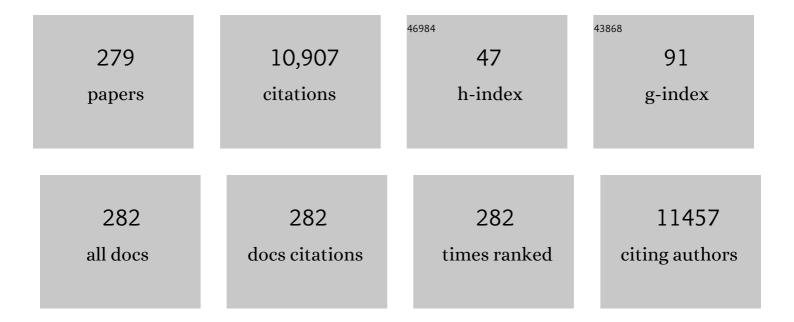
List of Publications by Year in descending order

Source: https://exaly.com/author-pdf/9603769/publications.pdf Version: 2024-02-01



#	Article	IF	CITATIONS
1	Perovskite light-emitting diodes with external quantum efficiency exceeding 20 per cent. Nature, 2018, 562, 245-248.	13.7	2,589
2	Strain control and spontaneous phase ordering in vertical nanocomposite heteroepitaxial thin films. Nature Materials, 2008, 7, 314-320.	13.3	334
3	Thick lead-free ferroelectric films with high Curie temperatures through nanocomposite-induced strain. Nature Nanotechnology, 2011, 6, 491-495.	15.6	220
4	Controlled Growth of a Large-Size 2D Selenium Nanosheet and Its Electronic and Optoelectronic Applications. ACS Nano, 2017, 11, 10222-10229.	7.3	189
5	Dielectric relaxation, resonance and scaling behaviors in Sr3Co2Fe24O41 hexaferrite. Scientific Reports, 2015, 5, 13645.	1.6	180
6	Tunable Lowâ€Field Magnetoresistance in (La _{0.7} Sr _{0.3} MnO ₃) _{0.5} :(ZnO) _{0.5} Selfâ€Assembled Vertically Aligned Nanocomposite Thin Films. Advanced Functional Materials, 2011, 21, 2423-2429.	7.8	174
7	Structural, electrical, and terahertz transmission properties of VO2 thin films grown on c-, r-, and m-plane sapphire substrates. Journal of Applied Physics, 2012, 111, .	1.1	172
8	Microstructure, vertical strain control and tunable functionalities in self-assembled, vertically aligned nanocomposite thin films. Acta Materialia, 2013, 61, 2783-2792.	3.8	153
9	Strongly enhanced oxygen ion transport through samarium-doped CeO2 nanopillars in nanocomposite films. Nature Communications, 2015, 6, 8588.	5.8	145
10	Making g-C3N4 ultra-thin nanosheets active for photocatalytic overall water splitting. Applied Catalysis B: Environmental, 2021, 282, 119557.	10.8	121
11	Why In ₂ O ₃ Can Make 0.7 nm Atomic Layer Thin Transistors. Nano Letters, 2021, 21, 500-506.	4.5	99
12	Interfacial coupling in heteroepitaxial vertically aligned nanocomposite thin films: From lateral to vertical control. Current Opinion in Solid State and Materials Science, 2014, 18, 6-18.	5.6	98
13	Scaled indium oxide transistors fabricated using atomic layer deposition. Nature Electronics, 2022, 5, 164-170.	13.1	98
14	Highâ€ \mathbf{S} trength Nanotwinned Al Alloys with 9R Phase. Advanced Materials, 2018, 30, 1704629.	11.1	93
15	High power density thin film SOFCs with YSZ/GDC bilayer electrolyte. Electrochimica Acta, 2011, 56, 5472-5477.	2.6	92
16	Self-Assembled Epitaxial Au–Oxide Vertically Aligned Nanocomposites for Nanoscale Metamaterials. Nano Letters, 2016, 16, 3936-3943.	4.5	91
17	lonic Conductivity Increased by Two Orders of Magnitude in Micrometer-Thick Vertical Yttria-Stabilized ZrO ₂ Nanocomposite Films. Nano Letters, 2015, 15, 7362-7369.	4.5	90
18	Vertical Interface Effect on the Physical Properties of Selfâ€Assembled Nanocomposite Epitaxial Films. Advanced Materials, 2009, 21, 3794-3798.	11.1	87

#	Article	IF	CITATIONS
19	Continuous Tuning of Phase Transition Temperature in VO ₂ Thin Films on <i>c</i> Cut Sapphire Substrates via Strain Variation. ACS Applied Materials & Interfaces, 2017, 9, 5319-5327.	4.0	87
20	High temperature deformability of ductile flash-sintered ceramics via in-situ compression. Nature Communications, 2018, 9, 2063.	5.8	87
21	New epitaxy paradigm in epitaxial self-assembled oxide vertically aligned nanocomposite thin films. Journal of Materials Research, 2017, 32, 4054-4066.	1.2	86
22	Nanoscale stacking fault–assisted room temperature plasticity in flash-sintered TiO ₂ . Science Advances, 2019, 5, eaaw5519.	4.7	82
23	Self-assembled oxide films with tailored nanoscale ionic and electronic channels for controlled resistive switching. Nature Communications, 2016, 7, 12373.	5.8	81
24	Role of scaffold network in controlling strain and functionalities of nanocomposite films. Science Advances, 2016, 2, e1600245.	4.7	80
25	A New Class of Roomâ€Temperature Multiferroic Thin Films with Bismuthâ€Based Supercell Structure. Advanced Materials, 2013, 25, 1028-1032.	11.1	78
26	Novel Electroformingâ€Free Nanoscaffold Memristor with Very High Uniformity, Tunability, and Density. Advanced Materials, 2014, 26, 6284-6289.	11.1	75
27	Extrinsic Green Photoluminescence from the Edges of 2D Cesium Lead Halides. Advanced Materials, 2019, 31, e1902492.	11.1	75
28	Microstructure, magnetic, and low-field magnetotransport properties of self-assembled (La _{0.7} Sr _{0.3} MnO ₃) _{0.5} :(CeO ₂) _{0.5} v aligned nanocomposite thin films. Nanotechnology, 2011, 22, 315712.	entically	70
29	Multifunctional, self-assembled oxide nanocomposite thin films and devices. MRS Bulletin, 2015, 40, 736-745.	1.7	70
30	Promoting effect of cyano groups attached on g-C3N4 nanosheets towards molecular oxygen activation for visible light-driven aerobic coupling of amines to imines. Journal of Catalysis, 2018, 366, 237-244.	3.1	68
31	High-velocity projectile impact induced 9R phase in ultrafine-grained aluminium. Nature Communications, 2017, 8, 1653.	5.8	66
32	Self-assembled Co–BaZrO ₃ nanocomposite thin films with ultra-fine vertically aligned Co nanopillars. Nanoscale, 2017, 9, 7970-7976.	2.8	64
33	Multifunctional La _{0.67} Sr _{0.33} MnO ₃ (LSMO) Thin Films Integrated on Mica Substrates toward Flexible Spintronics and Electronics. ACS Applied Materials & Interfaces, 2018, 10, 42698-42705.	4.0	62
34	Ultra-smooth glassy graphene thin films for flexible transparent circuits. Science Advances, 2016, 2, e1601574.	4.7	59
35	Integration of Self-Assembled Vertically Aligned Nanocomposite (La _{0.7} Sr _{0.3} MnO ₃) _{1–<i>x</i>} :(ZnO) _{<i>x</i>} Thin Films on Silicon Substrates. ACS Applied Materials & Interfaces, 2013, 5, 3995-3999.	4.0	58
36	Three-dimensional strain engineering in epitaxial vertically aligned nanocomposite thin films with	6.4	57

#	Article	IF	CITATIONS
37	Nanoscale Artificial Plasmonic Lattice in Selfâ€Assembled Vertically Aligned Nitride–Metal Hybrid Metamaterials. Advanced Science, 2018, 5, 1800416.	5.6	56
38	Selfâ€Assembled Ordered Threeâ€Phase Au–BaTiO ₃ –ZnO Vertically Aligned Nanocomposites Achieved by a Templating Method. Advanced Materials, 2019, 31, e1806529.	11.1	56
39	Strain Tuning and Strong Enhancement of Ionic Conductivity in SrZrO ₃ –RE ₂ O ₃ (RE = Sm, Eu, Gd, Dy, and Er) Nanocomposite Films. Advanced Functional Materials, 2015, 25, 4328-4333.	7.8	54
40	Highâ€speed atmospheric atomic layer deposition of ultra thin amorphous TiO ₂ blocking layers at 100 °C for inverted bulk heterojunction solar cells. Progress in Photovoltaics: Research and Applications, 2013, 21, 393-400.	4.4	52
41	Vertically aligned nanocomposite electrolytes with superior out-of-plane ionic conductivity for solid oxide fuel cells. Journal of Power Sources, 2013, 242, 455-463.	4.0	52
42	Sharp semiconductor-to-metal transition of VO2 thin films on glass substrates. Journal of Applied Physics, 2013, 114, .	1.1	52
43	Perovskite Transparent Conducting Oxide for the Design of a Transparent, Flexible, and Self-Powered Perovskite Photodetector. ACS Applied Materials & Interfaces, 2020, 12, 16462-16468.	4.0	52
44	Very High Surface Area Mesoporous Thin Films of SrTiO ₃ Grown by Pulsed Laser Deposition and Application to Efficient Photoelectrochemical Water Splitting. Nano Letters, 2016, 16, 7338-7345.	4.5	51
45	Couplings of Polarization with Interfacial Deep Trap and Schottky Interface Controlled Ferroelectric Memristive Switching. Advanced Functional Materials, 2020, 30, 2000664.	7.8	50
46	Precise Tuning of (YBa ₂ Cu ₃ O _{7â€Î´}) _{1â€x} :(BaZrO ₃) _x Thin Film Nanocomposite Structures. Advanced Functional Materials, 2014, 24, 5240-5245.	7.8	49
47	Roles of grain boundaries on the semiconductor to metal phase transition of VO2 thin films. Applied Physics Letters, 2015, 107, .	1.5	48
48	Ferroelectric Properties of Vertically Aligned Nanostructured BaTiO ₃ –CeO ₂ Thin Films and Their Integration on Silicon. ACS Applied Materials & Interfaces, 2013, 5, 12541-12547.	4.0	47
49	Strong room temperature exchange bias in self-assembled BiFeO3–Fe3O4 nanocomposite heteroepitaxial films. Applied Physics Letters, 2013, 102, .	1.5	46
50	Resonance Raman spectroscopy of G-line and folded phonons in twisted bilayer graphene with large rotation angles. Applied Physics Letters, 2013, 103, .	1.5	46
51	Laser-Induced Mesoporous Nickel Oxide as a Highly Sensitive Nonenzymatic Glucose Sensor. ACS Applied Nano Materials, 2020, 3, 5260-5270.	2.4	46
52	Strain relaxation and enhanced perpendicular magnetic anisotropy in BiFeO3:CoFe2O4 vertically aligned nanocomposite thin films. Applied Physics Letters, 2014, 104, .	1.5	45
53	The Role of Lattice Misfit on Heterogeneous Nucleation of Pure Aluminum. Metallurgical and Materials Transactions A: Physical Metallurgy and Materials Science, 2016, 47, 5012-5022.	1.1	45
54	Microstructural and magnetic properties of (La0.7Sr0.3MnO3)0.7:(Mn3O4)0.3 nanocomposite thin films. Journal of Applied Physics, 2011, 109, .	1.1	44

#	Article	IF	CITATIONS
55	The effects of external fields in ceramic sintering. Journal of the American Ceramic Society, 2019, 102, 5-31.	1.9	44
56	Strong perpendicular exchange bias in epitaxial La _{0.7} Sr _{0.3} MnO ₃ :BiFeO ₃ nanocomposite films through vertical interfacial coupling. Nanoscale, 2015, 7, 13808-13815.	2.8	43
57	Real-time in situ optical tracking of oxygen vacancy migration in memristors. Nature Electronics, 2020, 3, 687-693.	13.1	43
58	Rapid Upcycling of Waste Polyethylene Terephthalate to Energy Storing Disodium Terephthalate Flowers with DFT Calculations. ACS Sustainable Chemistry and Engineering, 2020, 8, 6252-6262.	3.2	43
59	Textured metastable VO2 (B) thin films on SrTiO3 substrates with significantly enhanced conductivity. Applied Physics Letters, 2014, 104, .	1.5	41
60	Perpendicular Exchange-Biased Magnetotransport at the Vertical Heterointerfaces in La _{0.7} Sr _{0.3} MnO ₃ :NiO Nanocomposites. ACS Applied Materials & Interfaces, 2015, 7, 21646-21651.	4.0	40
61	Bioinspired Dynamic Camouflage from Colloidal Nanocrystals Embedded Electrochromics. Nano Letters, 2021, 21, 4500-4507.	4.5	40
62	Self-Assembled Magnetic Metallic Nanopillars in Ceramic Matrix with Anisotropic Magnetic and Electrical Transport Properties. ACS Applied Materials & Interfaces, 2016, 8, 20283-20291.	4.0	39
63	Room Temperature Ferrimagnetism and Ferroelectricity in Strained, Thin Films of BiFe _{0.5} Mn _{0.5} O ₃ . Advanced Functional Materials, 2014, 24, 7478-7487.	7.8	38
64	Metal-Free Oxide-Nitride Heterostructure as a Tunable Hyperbolic Metamaterial Platform. Nano Letters, 2020, 20, 6614-6622.	4.5	38
65	New strain states and radical property tuning of metal oxides using a nanocomposite thin film approach. APL Materials, 2015, 3, 062507.	2.2	37
66	In situ polymerization of ethylenedioxythiophene from sulfonated carbon nanotube templates: toward high efficiency ITO-free solar cells. Journal of Materials Chemistry A, 2016, 4, 6645-6652.	5.2	37
67	Hybrid plasmonic Au–TiN vertically aligned nanocomposites: a nanoscale platform towards tunable optical sensing. Nanoscale Advances, 2019, 1, 1045-1054.	2.2	37
68	Tunable lattice strain in vertically aligned nanocomposite (BiFeO3)x:(Sm2O3)1â^'x thin films. Journal of Applied Physics, 2009, 106, .	1.1	36
69	Selfâ€Organized Epitaxial Vertically Aligned Nanocomposites with Longâ€Range Ordering Enabled by Substrate Nanotemplating. Advanced Materials, 2017, 29, 1606861.	11.1	36
70	Exchange Bias in a La _{0.67} Sr _{0.33} MnO ₃ /NiO Heterointerface Integrated on a Flexible Mica Substrate. ACS Applied Materials & Interfaces, 2020, 12, 39920-39925.	4.0	36
71	Solar-Blind UV Photodetector Based on Atomic Layer-Deposited Cu ₂ O and Nanomembrane β-Ga ₂ O ₃ pn Oxide Heterojunction. ACS Omega, 2019, 4, 20756-20761.	1.6	35
72	Tailorable Au Nanoparticles Embedded in Epitaxial TiO ₂ Thin Films for Tunable Optical Properties. ACS Applied Materials & Interfaces, 2018, 10, 32895-32902.	4.0	34

#	Article	IF	CITATIONS
73	Self-assembled vertically aligned Ni nanopillars in CeO ₂ with anisotropic magnetic and transport properties for energy applications. Nanoscale, 2018, 10, 17182-17188.	2.8	34
74	Evolution of microstructure, strain and physical properties in oxide nanocomposite films. Scientific Reports, 2014, 4, 5426.	1.6	33
75	Exchange Bias Effect along Vertical Interfaces in La0.7Sr0.3MnO3:NiO Vertically Aligned Nanocomposite Thin Films Integrated on Silicon Substrates. Crystal Growth and Design, 2018, 18, 4388-4394.	1.4	33
76	Tailorable Optical Response of Au–LiNbO ₃ Hybrid Metamaterial Thin Films for Optical Waveguide Applications. Advanced Optical Materials, 2018, 6, 1800510.	3.6	32
77	High strength, deformable nanotwinned Al–Co alloys. Materials Research Letters, 2019, 7, 33-39.	4.1	32
78	Study of the Flux Pinning Landscape of YBCO Thin Films With Single and Mixed Phase Additions BaMO3 + Z: M = Hf, Sn, Zr and Z = Y2O3, Y211. IEEE Transactions on Applied Superconductivity, 2017, 27, 1-5.	1.1	31
79	3D strain-induced superconductivity in La ₂ CuO _{4+δ} using a simple vertically aligned nanocomposite approach. Science Advances, 2019, 5, eaav5532.	4.7	31
80	Selfâ€Assembled Ag–TiN Hybrid Plasmonic Metamaterial: Tailorable Tilted Nanopillar and Optical Properties. Advanced Optical Materials, 2019, 7, 1801180.	3.6	31
81	Engineered heat dissipation and current distribution boron nitride-graphene layer coated on polypropylene separator for high performance lithium metal battery. Journal of Colloid and Interface Science, 2021, 583, 362-370.	5.0	31
82	Role of ALD Al ₂ O ₃ Surface Passivation on the Performance of p-Type Cu ₂ O Thin Film Transistors. ACS Applied Materials & Interfaces, 2021, 13, 4156-4164.	4.0	31
83	A New Material for Highâ€Temperature Leadâ€Free Actuators. Advanced Functional Materials, 2013, 23, 5881-5886.	7.8	30
84	Plastic deformation mechanisms and size effect of Cu50Zr50/Cu amorphous/crystalline nanolaminate: A molecular dynamics study. Computational Materials Science, 2017, 129, 137-146.	1.4	30
85	Strain-induced suppression of the miscibility gap in nanostructured Mg ₂ Si–Mg ₂ Sn solid solutions. Journal of Materials Chemistry A, 2018, 6, 17559-17570.	5.2	30
86	Strain-driven nanodumbbell structure and enhanced physical properties in hybrid vertically aligned nanocomposite thin films. Applied Materials Today, 2019, 16, 204-212.	2.3	30
87	Strain-Driven In-plane Ordering in Vertically Aligned ZnO–Au Nanocomposites with Highly Correlated Metamaterial Properties. ACS Omega, 2020, 5, 2234-2241.	1.6	30
88	Research Updates: Epitaxial strain relaxation and associated interfacial reconstructions: The driving force for creating new structures with integrated functionality. APL Materials, 2013, 1, .	2.2	29
89	LiNi0.5Mn0.3Co0.2O2/Au nanocomposite thin film cathode with enhanced electrochemical properties. Nano Energy, 2018, 46, 290-296.	8.2	29
90	Vertically Aligned Nanocomposite BaTiO ₃ :YMnO ₃ Thin Films with Room Temperature Multiferroic Properties toward Nanoscale Memory Devices. ACS Applied Nano Materials, 2018, 1, 2509-2514.	2.4	29

#	Article	IF	CITATIONS
91	Self-Assembled Heteroepitaxial Oxide Nanocomposite for Photoelectrochemical Solar Water Oxidation. Chemistry of Materials, 2016, 28, 3017-3023.	3.2	28
92	Practical Magnetic Pinning in YBCO. IEEE Transactions on Applied Superconductivity, 2009, 19, 3148-3151.	1.1	27
93	Microscopic adaptation of BaHfO ₃ and Y ₂ O ₃ artificial pinning centers for strong and isotropic pinning landscape in YBa ₂ Cu ₃ O _{7–<i>x</i>} thin films. Superconductor Science and Technology. 2018. 31. 025008.	1.8	27
94	Tunable Optical Properties in Selfâ€Assembled Oxideâ€Metal Hybrid Thin Films via Auâ€Phase Geometry Control: From Nanopillars to Nanodisks. Advanced Optical Materials, 2020, 8, 1901359.	3.6	27
95	Highly Conductive Copper–Silver Bimodal Paste for Low-Cost Printed Electronics. ACS Applied Electronic Materials, 2021, 3, 3352-3364.	2.0	27
96	Enhanced tunable magnetoresistance properties over a wide temperature range in epitaxial (La0.7Sr0.3MnO3)1â~x:(CeO2)x nanocomposites. Journal of Applied Physics, 2015, 118, .	1.1	26
97	Aqueous Solution-Deposited Molybdenum Oxide Films as an Anode Interfacial Layer for Organic Solar Cells. ACS Applied Materials & Interfaces, 2015, 7, 18218-18224.	4.0	26
98	Two-Dimensional Layered Oxide Structures Tailored by Self-Assembled Layer Stacking via Interfacial Strain. ACS Applied Materials & Interfaces, 2016, 8, 16845-16851.	4.0	26
99	Broad Range Tuning of Phase Transition Property in VO ₂ Through Metal eramic Nanocomposite Design. Advanced Functional Materials, 2019, 29, 1903690.	7.8	26
100	Multifunctional Metal–Oxide Nanocomposite Thin Film with Plasmonic Au Nanopillars Embedded in Magnetic La _{0.67} Sr _{0.33} MnO ₃ Matrix. Nano Letters, 2021, 21, 1032-1039.	4.5	26
101	A simplified superconducting coated conductor design with Fe-based superconductors on glass and flexible metallic substrates. Journal of Alloys and Compounds, 2015, 647, 380-385.	2.8	25
102	Turning antiferromagnetic Sm _{0.34} Sr _{0.66} MnO ₃ into a 140 K ferromagnet using a nanocomposite strain tuning approach. Nanoscale, 2016, 8, 8083-8090.	2.8	25
103	Novel Layered Supercell Structure from Bi ₂ AlMnO ₆ for Multifunctionalities. Nano Letters, 2017, 17, 6575-6582.	4.5	25
104	Integration of Hybrid Plasmonic Au–BaTiO ₃ Metamaterial on Silicon Substrates. ACS Applied Materials & Interfaces, 2019, 11, 45199-45206.	4.0	25
105	Study of deformation mechanisms in flash-sintered yttria-stabilized zirconia by <i>in-situ</i> micromechanical testing at elevated temperatures. Materials Research Letters, 2019, 7, 194-202.	4.1	25
106	Nitrideâ€Oxideâ€Metal Heterostructure with Selfâ€Assembled Core–Shell Nanopillar Arrays: Effect of Ordering on Magnetoâ€Optical Properties. Small, 2021, 17, e2007222.	5.2	25
107	A new approach to investigate Li ₂ MnO ₃ and Li(Ni _{0.5} Mn _{0.3} Co _{0.2})O ₂ mixed phase cathode materials. Journal of Materials Chemistry A, 2014, 2, 2283-2289.	5.2	24
108	Roles of strain and domain boundaries on the phase transition stability of VO2 thin films. Applied Physics Letters, 2017, 111, .	1.5	24

#	Article	IF	CITATIONS
109	"Ductile―Fracture of Metallic Glass Nanolaminates. Advanced Materials Interfaces, 2017, 4, 1700510.	1.9	24
110	Microstructure, Magnetic, and Magnetoresistance Properties of La0.7Sr0.3MnO3:CuO Nanocomposite Thin Films. ACS Applied Materials & Interfaces, 2018, 10, 5779-5784.	4.0	24
111	Design of a Vertical Composite Thin Film System with Ultralow Leakage To Yield Large Converse Magnetoelectric Effect. ACS Applied Materials & Interfaces, 2018, 10, 18237-18245.	4.0	24
112	Interface Engineered Roomâ€Temperature Ferromagnetic Insulating State in Ultrathin Manganite Films. Advanced Science, 2020, 7, 1901606.	5.6	24
113	Flash sintering incubation kinetics. Npj Computational Materials, 2020, 6, .	3.5	24
114	Overcoming the Anisotropic Growth Limitations of Freeâ€Standing Singleâ€Crystal Halide Perovskite Films. Angewandte Chemie - International Edition, 2021, 60, 2629-2636.	7.2	24
115	Defects in flash-sintered ceramics and their effects on mechanical properties. MRS Bulletin, 2021, 46, 44-51.	1.7	24
116	Monolithic Mid-Infrared Integrated Photonics Using Silicon-on-Epitaxial Barium Titanate Thin Films. ACS Applied Materials & Interfaces, 2017, 9, 21848-21855.	4.0	23
117	Review on the growth, properties and applications of self-assembled oxide–metal vertically aligned nanocomposite thin films—current and future perspectives. Materials Horizons, 2021, 8, 869-884.	6.4	23
118	Wireless Humidity Sensor for Smart Packaging via Oneâ€step Laserâ€Induced Patterning and Nanoparticle Formation on Metallized Paper. Advanced Electronic Materials, 2022, 8, .	2.6	23
119	Emergent multiferroism with magnetodielectric coupling in EuTiO3 created by a negative pressure control of strong spin-phonon coupling. Nature Communications, 2022, 13, 2364.	5.8	23
120	Role of boundaries on low-field magnetotransport properties of La _{0.7} Sr _{0.3} MnO ₃ -based nanocomposite thin films. Journal of Materials Research, 2013, 28, 1707-1714.	1.2	22
121	Strain and Interface Effects in a Novel Bismuth-Based Self-Assembled Supercell Structure. ACS Applied Materials & Interfaces, 2015, 7, 11631-11636.	4.0	22
122	Strong perpendicular exchange bias in epitaxial La0.7Sr0.3MnO3:LaFeO3 nanocomposite thin films. APL Materials, 2016, 4, .	2.2	22
123	Probing the effect of interface on vortex pinning efficiency of one-dimensional BaZrO3 and BaHfO3 artificial pinning centers in YBa2Cu3O7-x thin films. Applied Physics Letters, 2018, 113, .	1.5	22
124	Spontaneous Ordering of Oxide-Oxide Epitaxial Vertically Aligned Nanocomposite Thin Films. Annual Review of Materials Research, 2020, 50, 229-253.	4.3	22
125	Advanced Thin Film Cathodes for Lithium Ion Batteries. Research, 2020, 2020, 2969510.	2.8	22
126	Vertical Interface Induced Dielectric Relaxation in Nanocomposite (BaTiO3)1-x:(Sm2O3)x Thin Films. Scientific Reports, 2015, 5, 11335.	1.6	21

#	Article	IF	CITATIONS
127	Mixed-Valence Perovskite Thin Films by Polymer-Assisted Deposition. Journal of the American Ceramic Society, 2008, 91, 1858-1863.	1.9	20
128	Transformational dynamics of BZO and BHO nanorods imposed by Y2O3 nanoparticles for improved isotropic pinning in YBa2Cu3O7-δ thin films. AIP Advances, 2017, 7, .	0.6	20
129	Vertically Aligned Ag _{<i>x</i>} Au _{1–<i>x</i>} Alloyed Nanopillars Embedded in ZnO as Nanoengineered Low-Loss Hybrid Plasmonic Metamaterials. Nano Letters, 2020, 20, 3778-3785.	4.5	20
130	Carbon Nanotube Supported Amorphous MoS ₂ via Microwave Heating Synthesis for Enhanced Performance of Hydrogen Evolution Reaction. Energy Material Advances, 2021, 2021, .	4.7	20
131	Structure and magnetotransport properties of epitaxial nanocomposite La0.67Ca0.33MnO3:SrTiO3 thin films grown by a chemical solution approach. Applied Physics Letters, 2012, 100, 082403.	1.5	19
132	Effective magnetic pinning schemes for enhanced superconducting property in high temperature superconductor YBa ₂ Cu ₃ O _{7â^'<i>x</i>} : a review. Superconductor Science and Technology, 2017, 30, 114004.	1.8	19
133	Real-Time and Label-Free Chemical Sensor-on-a-chip using Monolithic Si-on-BaTiO3 Mid-Infrared waveguides. Scientific Reports, 2017, 7, 5836.	1.6	19
134	Enhancing electrochemical performance of thin film lithium ion battery via introducing tilted metal nanopillars as effective current collectors. Nano Energy, 2020, 69, 104381.	8.2	18
135	3D Hybrid Plasmonic Framework with Au Nanopillars Embedded in Nitride Multilayers Integrated on Si. Advanced Materials Interfaces, 2020, 7, 2000493.	1.9	18
136	Self-biased magnetoelectric switching at room temperature in three-phase ferroelectric–antiferromagnetic–ferrimagnetic nanocomposites. Nature Electronics, 2021, 4, 333-341.	13.1	18
137	Printing dynamic color palettes and layered textures through modeling-guided stacking of electrochromic polymers. Materials Horizons, 2022, 9, 425-432.	6.4	18
138	Microstructural and Pinning Properties of \${m YBa}_{2}{m Cu}_{3}{m O}_{7-delta}\$ Thin Films Doped With Magnetic Nanoparticles. IEEE Transactions on Applied Superconductivity, 2009, 19, 3503-3506.	1.1	17
139	Room temperature mechanical behaviour of a Ni-Fe multilayered material with modulated grain size distribution. Philosophical Magazine, 2014, 94, 3549-3559.	0.7	17
140	Tailoring plasticity of metallic glasses via interfaces in Cu/amorphous CuNb laminates. Journal of Materials Research, 2017, 32, 2680-2689.	1.2	17
141	Strain Enhanced Functionality in a Bottomâ€Up Approach Enabled 3D Superâ€Nanocomposites. Advanced Functional Materials, 2019, 29, 1900442.	7.8	17
142	Multifunctional self-assembled BaTiO3-Au nanocomposite thin films on flexible mica substrates with tunable optical properties. Applied Materials Today, 2020, 21, 100856.	2.3	17
143	Nanoengineering room temperature ferroelectricity into orthorhombic SmMnO3 films. Nature Communications, 2020, 11, 2207.	5.8	17
144	Design of 3D Oxide–Metal Hybrid Metamaterial for Tailorable Light–Matter Interactions in Visible and Nearâ€Infrared Region. Advanced Optical Materials, 2021, 9, .	3.6	17

#	Article	IF	CITATIONS
145	High-Temperature and Flexible Piezoelectric Sensors for Lamb-Wave-Based Structural Health Monitoring. ACS Applied Materials & Interfaces, 2021, 13, 47764-47772.	4.0	17
146	Enhanced Flux Pinning Properties in Self-Assembled Magnetic \$hbox{CoFe}_{2}hbox{O}_{4}\$ Nanoparticles Doped \$ hbox{YBa}_{2}hbox{Cu}_{3}hbox{O}_{7 - delta}\$ Thin Films. IEEE Transactions on Applied Superconductivity, 2013, 23, 8001204-8001204.	1.1	16
147	Enhancement of Low-field Magnetoresistance in Self-Assembled Epitaxial La0.67Ca0.33MnO3:NiO and La0.67Ca0.33MnO3:Co3O4 Composite Films via Polymer-Assisted Deposition. Scientific Reports, 2016, 6, 26390.	1.6	16
148	Tunable magnetic anisotropy of self-assembled Fe nanostructures within a La0.5Sr0.5FeO3 matrix. Applied Physics Letters, 2018, 112, .	1.5	16
149	Oxygen-vacancy-mediated dielectric property in perovskite Eu0.5Ba0.5TiO3-δ epitaxial thin films. Applied Physics Letters, 2018, 112, .	1.5	16
150	All-Oxide Nanocomposites to Yield Large, Tunable Perpendicular Exchange Bias above Room Temperature. ACS Applied Materials & Interfaces, 2018, 10, 42593-42602.	4.0	16
151	Au-Encapsulated Fe Nanorods in Oxide Matrix with Tunable Magneto-Optic Coupling Properties. ACS Applied Materials & Interfaces, 2020, 12, 51827-51836.	4.0	16
152	Electrochromic Properties of Perovskite NdNiO ₃ Thin Films for Smart Windows. ACS Applied Electronic Materials, 2021, 3, 1719-1731.	2.0	16
153	A Biodegradable Hybrid Micro/Nano Conductive Zinc Paste for Paperâ€Based Flexible Bioelectronics. Advanced Materials Technologies, 2022, 7, .	3.0	16
154	Strongly Biasâ€Dependent Tunnel Magnetoresistance in Manganite Spin Filter Tunnel Junctions. Advanced Materials, 2015, 27, 3079-3084.	11.1	15
155	Strengthening mechanisms and deformability of nanotwinned AlMg alloys. Journal of Materials Research, 2018, 33, 3739-3749.	1.2	15
156	Tunable low-field magnetoresistance properties in (La0.7Ca0.3MnO3)1â^'x:(CeO2)x vertically aligned nanocomposite thin films. Applied Physics Letters, 2019, 115, 053103.	1.5	15
157	Tuning magnetic anisotropy in Co–BaZrO ₃ vertically aligned nanocomposites for memory device integration. Nanoscale Advances, 2019, 1, 4450-4458.	2.2	15
158	Vertically aligned nanocomposite (BaTiO ₃) _{0.8} : (La _{0.7} Sr _{0.3} MnO ₃) <su thin films with anisotropic multifunctionalities. Nanoscale Advances, 2020, 2, 3276-3283.</su 	b> 022 <td>b> 15</td>	b> 15
159	Thermally Stable Au–BaTiO ₃ Nanoscale Hybrid Metamaterial for High-Temperature Plasmonic Applications. ACS Applied Nano Materials, 2020, 3, 1431-1437.	2.4	15
160	Ferroelectric/multiferroic self-assembled vertically aligned nanocomposites: Current and future status. APL Materials, 2021, 9, .	2.2	15
161	Heteroepitaxy of flexible piezoelectric Pb(Zr0.53Ti0.47)O3 sensor on inorganic mica substrate for lamb wave-based structural health monitoring. Ceramics International, 2021, 47, 13156-13163.	2.3	15
162	Flux Pinning Properties in YBCO Thin Films With Self-Aligned Magnetic Nanoparticles. IEEE Transactions on Applied Superconductivity, 2011, 21, 2749-2752.	1.1	14

#	Article	IF	CITATIONS
163	Interfacial defects distribution and strain coupling in the vertically aligned nanocomposite YBa ₂ Cu ₃ O _{7-X} / BaSnO ₃ thin films. Journal of Materials Research, 2012, 27, 1763-1769.	1.2	14
164	Misfit paradox on nucleation potency of MgO and MgAl2O4 for Al. Materials Characterization, 2016, 119, 92-98.	1.9	14
165	Interfaceâ€Coupled BiFeO ₃ /BiMnO ₃ Superlattices with Magnetic Transition Temperature up to 410 K. Advanced Materials Interfaces, 2016, 3, 1500597.	1.9	14
166	Multiferroic vertically aligned nanocomposite with CoFe2O4 nanocones embedded in layered Bi2WO6 matrix. Materials Research Letters, 2019, 7, 418-425.	4.1	14
167	An in situ study on Kr ion–irradiated crystalline Cu/amorphous-CuNb nanolaminates. Journal of Materials Research, 2019, 34, 2218-2228.	1.2	14
168	Morphology Control of Self-Assembled Three-Phase Au-BaTiO ₃ –ZnO Hybrid Metamaterial for Tunable Optical Properties. Crystal Growth and Design, 2020, 20, 6101-6108.	1.4	14
169	Vertical Strain-Driven Antiferromagnetic to Ferromagnetic Phase Transition in EuTiO ₃ Nanocomposite Thin Films. ACS Applied Materials & Interfaces, 2020, 12, 8513-8521.	4.0	14
170	Core-shell metallic alloy nanopillars-in-dielectric hybrid metamaterials with magneto-plasmonic coupling. Materials Today, 2021, 51, 39-47.	8.3	14
171	In situ nanomechanical testing of twinned metals in a transmission electron microscope. MRS Bulletin, 2016, 41, 305-313.	1.7	13
172	Dual Beam In Situ Radiation Studies of Nanocrystalline Cu. Materials, 2019, 12, 2721.	1.3	13
173	Integration of highly anisotropic multiferroic BaTiO3–Fe nanocomposite thin films on Si towards device applications. Nanoscale Advances, 2020, 2, 4172-4178.	2.2	13
174	Bidirectional tuning of phase transition properties in Pt : VO ₂ nanocomposite thin films. Nanoscale, 2020, 12, 17886-17894.	2.8	13
175	Ultra-high heating rate effects on the sintering of ceramic nanoparticles: an <i>inÂsitu</i> TEM study. Materials Research Letters, 2021, 9, 373-381.	4.1	13
176	High-strength nanocrystalline intermetallics with room temperature deformability enabled by nanometer thick grain boundaries. Science Advances, 2021, 7, .	4.7	13
177	Laser-Assisted Nanotexturing and Silver Immobilization on Titanium Implant Surfaces to Enhance Bone Cell Mineralization and Antimicrobial Properties. Langmuir, 2022, 38, 4014-4027.	1.6	13
178	Nanoporous thin films with controllable nanopores processed from vertically aligned nanocomposites. Nanotechnology, 2010, 21, 285606.	1.3	12
179	Biopolymer mediated synthesis of plate-like YBCO with enhanced grain connectivity and intragranular critical current. CrystEngComm, 2012, 14, 5765.	1.3	12
180	Atomicâ€Scale Control of Electronic Structure and Ferromagnetic Insulating State in Perovskite Oxide Superlattices by Longâ€Range Tuning of BO ₆ Octahedra. Advanced Functional Materials, 2020, 30, 2001984.	7.8	12

#	Article	IF	CITATIONS
181	Self-assembled nitride–metal nanocomposites: recent progress and future prospects. Nanoscale, 2020, 12, 20564-20579.	2.8	12
182	Selfâ€Assembled Metal–Dielectric Hybrid Metamaterials in Vertically Aligned Nanocomposite Form with Tailorable Optical Properties and Coupled Multifunctionalities. Advanced Photonics Research, 2021, 2, 2000174.	1.7	12
183	Flash sintering of additively manufactured 3YSZ gears. Journal of the American Ceramic Society, 2021, 104, 3828-3832.	1.9	12
184	Enhancing magnetic pinning by BaZrO ₃ nanorods forming coherent interface by strain-directed Ca-doping in YBa ₂ Cu ₃ O _{7â^'x} nanocomposite films. Superconductor Science and Technology, 2021, 34, 104002.	1.8	12
185	Atomic interface sequence, misfit strain relaxation and intrinsic flux-pinning defects in different YBa ₂ Cu ₃ O _{7â^îl} heterogeneous systems. Superconductor Science and Technology, 2013, 26, 025009.	1.8	11
186	Thermal stability of amorphous SiOC/crystalline Fe composite. Philosophical Magazine, 2015, 95, 3876-3887.	0.7	11
187	Room temperature magnetodielectric effects in epitaxial hexaferrite BaFe10.2Sc1.8O19 thin film. Applied Physics Letters, 2017, 110, .	1.5	11
188	Li ₂ MnO ₃ Thin Films with Tilted Domain Structure as Cathode for Li-Ion Batteries. ACS Applied Energy Materials, 2019, 2, 3461-3468.	2.5	11
189	Fieldâ€assisted heating of Gdâ€doped ceria thin film. Journal of the American Ceramic Society, 2020, 103, 2309-2314.	1.9	11
190	Anisotropic domains and antiferrodistortive-transition controlled magnetization in epitaxial manganite films on vicinal SrTiO3 substrates. Applied Physics Letters, 2020, 117, .	1.5	11
191	Negative-pressure enhanced ferroelectricity and piezoelectricity in lead-free BaTiO ₃ ferroelectric nanocomposite films. Journal of Materials Chemistry C, 2020, 8, 8091-8097.	2.7	11
192	Preparative Mass Spectrometry Using a Rotatingâ€Wall Mass Analyzer. Angewandte Chemie - International Edition, 2020, 59, 7711-7716.	7.2	11
193	Novel layered Bi ₃ MoM _T O ₉ (M _T = Mn, Fe, Co and Ni) thin films with tunable multifunctionalities. Nanoscale, 2020, 12, 5914-5921.	2.8	11
194	Largeâ€Scale Plasmonic Hybrid Framework with Builtâ€In Nanohole Array as Multifunctional Optical Sensing Platforms. Small, 2020, 16, 1906459.	5.2	11
195	Integration of Highly Luminescent Lead Halide Perovskite Nanocrystals on Transparent Lead Halide Nanowire Waveguides through Morphological Transformation and Spontaneous Growth in Water. Small, 2022, 18, e2105009.	5.2	11
196	Freestanding La _{0.7} Sr _{0.3} MnO ₃ :NiO vertically aligned nanocomposite thin films for flexible perpendicular interfacial exchange coupling. Materials Research Letters, 2022, 10, 287-294.	4.1	11
197	Giant Enhancement of Polarization and Strong Improvement of Retention in Epitaxial Ba _{0.6} Sr _{0.4} TiO ₃ â€Based Nanocomposites. Advanced Materials Interfaces, 2017, 4, 1700336.	1.9	10
198	Use of Mesoscopic Host Matrix to Induce Ferrimagnetism in Antiferromagnetic Spinel Oxide. Advanced Functional Materials, 2018, 28, 1706220.	7.8	10

#	Article	IF	CITATIONS
199	Tunable physical properties in BiAl _{1â^x} Mn _x O ₃ thin films with novel layered supercell structures. Nanoscale Advances, 2020, 2, 315-322.	2.2	10
200	Substrate oxygen sponge effect: A parameter for epitaxial manganite thin film growth. Applied Physics Letters, 2020, 117, .	1.5	10
201	Engineering lithium-ion battery cathodes for high-voltage applications using electromagnetic excitation. Journal of Materials Science, 2020, 55, 12177-12190.	1.7	10
202	Epitaxial TiN/MgO multilayers with ultrathin TiN and MgO layers as hyperbolic metamaterials in visible region. Materials Today Physics, 2021, 16, 100316.	2.9	10
203	High performance, electroforming-free, thin film memristors using ionic Na _{0.5} Bi _{0.5} TiO ₃ . Journal of Materials Chemistry C, 2021, 9, 4522-4531.	2.7	10
204	Ultrathin epitaxial NbN superconducting films with high upper critical field grown at low temperature. Materials Research Letters, 2021, 9, 336-342.	4.1	10
205	High stability of flexible perovskite transparent conductive oxide film via van der Waals heteroepitaxy. Journal of Alloys and Compounds, 2022, 890, 161897.	2.8	10
206	High ionic conductivity in fluorite δ-bismuth oxide-based vertically aligned nanocomposite thin films. Journal of Materials Chemistry A, 2022, 10, 3478-3484.	5.2	10
207	Role of Defects and Power Dissipation on Ferroelectric Memristive Switching. Advanced Electronic Materials, 2022, 8, .	2.6	10
208	Study of \${m Sm}_{m x}{m Zr}_{1-{m x}}{m O}_{m y}\$ Buffer Layer and Its Effects on YBCO Properties. IEEE Transactions on Applied Superconductivity, 2007, 17, 3409-3412.	1.1	9
209	Cubic HfN Thin Films with Low Resistivity on Si (001) and MgO (001) Substrates. Journal of Electronic Materials, 2008, 37, 1828-1831.	1.0	9
210	Correlation Between Flux Pinning Properties and Interfacial Defects in \${m YBa}_{2}{m Cu}_{3}{m O}_{7-delta}/{m CeO}_{2}\$ Multilayer Thin Films. IEEE Transactions on Applied Superconductivity, 2011, 21, 2758-2761.	1.1	9
211	Two-Phase Room-Temperature Multiferroic Nanocomposite with BiMnO3-Tilted Nanopillars in the Bi2W1–xMnxO6 Matrix. ACS Applied Materials & Interfaces, 2019, 11, 26261-26267.	4.0	9
212	3D Hybrid Trilayer Heterostructure: Tunable Au Nanorods and Optical Properties. ACS Applied Materials & Interfaces, 2020, 12, 45015-45022.	4.0	9
213	Route to High-Performance Micro-solid Oxide Fuel Cells on Metallic Substrates. ACS Applied Materials & Interfaces, 2021, 13, 4117-4125.	4.0	9
214	Novel vertically aligned nanocomposite of Bi2WO6-Co3O4 with room-temperature multiferroic and anisotropic optical response. Nano Research, 0, , 1.	5.8	9
215	High Strength and Low Coercivity of Cobalt with Three-Dimensional Nanoscale Stacking Faults. Nano Letters, 2021, 21, 6480-6486.	4.5	9
216	Ordered hybrid metamaterial of La0.7Sr0.3MnO3–Au vertically aligned nanocomposites achieved on templated SrTiO3 substrate. Materials Today Nano, 2021, 15, 100121.	2.3	9

#	Article	IF	CITATIONS
217	Stabilizing new bismuth compounds in thin film form. Journal of Materials Research, 2016, 31, 3530-3537.	1.2	8
218	Superconducting Iron Chalcogenide Thin Films Integrated on Flexible Mica Substrates. IEEE Transactions on Applied Superconductivity, 2019, 29, 1-4.	1.1	8
219	Breaking Lattice Symmetry in Highly Strained Epitaxial VO ₂ Films on Faceted Nanosurface. ACS Applied Materials & Interfaces, 2019, 11, 44905-44912.	4.0	8
220	Self-Assembled BaTiO ₃ –Au <i>_x</i> Ag _{1–<i>x</i>} Low-Loss Hybrid Plasmonic Metamaterials with an Ordered "Nano-Domino-like―Microstructure. ACS Applied Materials & Interfaces, 2021, 13, 5390-5398.	4.0	8
221	Electrical properties and charge compensation mechanisms of Cr-doped rutile, TiO ₂ . Physical Chemistry Chemical Physics, 2021, 23, 22133-22146.	1.3	8
222	Strong pinning at high growth rates in rare earth barium cuprate (REBCO) superconductor films grown with liquid-assisted processing (LAP) during pulsed laser deposition. Superconductor Science and Technology, 2021, 34, 045012.	1.8	8
223	Nanocomposite‧eeded Epitaxial Growth of Singleâ€Domain Lithium Niobate Thin Films for Surface Acoustic Wave Devices. Advanced Photonics Research, 2021, 2, 2000149.	1.7	8
224	Origin of High Interfacial Resistance in Solid‣tate Batteries: LLTO/LCO Half ells**. ChemElectroChem, 2021, 8, 1847-1857.	1.7	8
225	Electroforming-Free HfO ₂ :CeO ₂ Vertically Aligned Nanocomposite Memristors with Anisotropic Dielectric Response. ACS Applied Electronic Materials, 2021, 3, 5278-5286.	2.0	8
226	Enabling coherent BaZrO ₃ nanorods/YBa ₂ Cu ₃ O _{7â^x} interface through dynamic lattice enlargement in vertical epitaxy of BaZrO ₃ /YBa ₂ Cu ₃ O _{7â^x} nanocomposites.	1.8	8
227	Superconductor Science and Technology, 2022, 35, 034001. Enhanced Flux Pinning Properties of YBCO Thin Films With Various Pinning Landscapes. IEEE Transactions on Applied Superconductivity, 2017, 27, 1-5.	1.1	7
228	Constitutive analysis and optimization on hot working parameters of as-cast high Cr ultra-super-critical rotor steel with columnar grains. Journal of Iron and Steel Research International, 2017, 24, 916-924.	1.4	7
229	Strategies to tailor serrated flows in metallic glasses. Journal of Materials Research, 2019, 34, 1595-1607.	1.2	7
230	Comparison Study of the Flux Pinning Enhancement of YBa ₂ Cu ₃ O _{7â^{^*}Î′} Thin Films With BaHfO ₃ + Y ₂ O ₃ Single- and Mixed-Phase Additions. IEEE Transactions on Applied Superconductivity, 2019, 29, 1-5.	1.1	7
231	Titanium Nitride Modified Photoluminescence from Single Semiconductor Nanoplatelets. Advanced Functional Materials, 2020, 30, 1904179.	7.8	7
232	Ceramic Material Processing Towards Future Space Habitat: Electric Current-Assisted Sintering of Lunar Regolith Simulant. Materials, 2020, 13, 4128.	1.3	7
233	Role of Interlayer in 3D Vertically Aligned Nanocomposite Frameworks with Tunable Magnetotransport Properties. Advanced Materials Interfaces, 2020, 7, 1901990.	1.9	7
234	Deposition pressure-induced microstructure control and plasmonic property tuning in hybrid ZnO–Ag _x Au _{1â^'x} thin films. Nanoscale Advances, 2021, 3, 2870-2878.	2.2	7

#	Article	IF	CITATIONS
235	Strong Interfacial Coupling of Tunable Ni–NiO Nanocomposite Thin Films Formed by Self-Decomposition. ACS Applied Materials & Interfaces, 2021, 13, 39730-39737.	4.0	7
236	Tunable Three-Phase Co–CeO ₂ –BaTiO ₃ Hybrid Metamaterials with Nano-Mushroom-Like Structure for Tailorable Multifunctionalities. ACS Applied Nano Materials, 2022, 5, 6297-6304.	2.4	7
237	Vertically stacked multilayer atomic-layer-deposited sub-1-nm In2O3 field-effect transistors with back-end-of-line compatibility. Applied Physics Letters, 2022, 120, .	1.5	7
238	Tunable physical properties in Bi-based layered supercell multiferroics embedded with Au nanoparticles. Nanoscale Advances, 2022, 4, 3054-3064.	2.2	7
239	Interfacial Defects and Flux-Pinning Effects in Nanostructured \${m YBa}_{2}{m Cu}_{3}{m O}_{7-delta}\$ Thin Films. IEEE Transactions on Applied Superconductivity, 2009, 19, 3395-3398.	1.1	6
240	Growth and Pinning Properties of Superconducting Nanostructured \$hbox{FeSe}_{0.5}hbox{Te}_{0.5}\$ Thin Films on Amorphous Substrates. IEEE Transactions on Applied Superconductivity, 2013, 23, 7500904-7500904.	1.1	6
241	Interfacial Engineering Enabled Novel Bi-Based Layered Oxide Supercells with Modulated Microstructures and Tunable Physical Properties. Crystal Growth and Design, 2019, 19, 7088-7095.	1.4	6
242	Defectâ€Mediated Anisotropic Lattice Expansion in Ceramics as Evidence for Nonthermal Coupling between Electromagnetic Fields and Matter. Advanced Engineering Materials, 2019, 21, 1900762.	1.6	6
243	AlN-based hybrid thin films with self-assembled plasmonic Au and Ag nanoinclusions. Applied Physics Letters, 2019, 114, .	1.5	6
244	Room-Temperature Ferroelectric LiNb ₆ Ba ₅ Ti ₄ O ₃₀ Spinel Phase in a Nanocomposite Thin Film Form for Nonlinear Photonics. ACS Applied Materials & Interfaces, 2020, 12, 23076-23083.	4.0	6
245	Double-Exchange Bias Modulation under Horizontal and Perpendicular Field Directions by 3D Nanocomposite Design. ACS Applied Materials & Interfaces, 2021, 13, 50141-50148.	4.0	6
246	Self-assembled vertically aligned nanocomposite systems integrated on silicon substrate: Progress and future perspectives. Journal of Vacuum Science and Technology A: Vacuum, Surfaces and Films, 2022, 40, .	0.9	6
247	Epitaxial (110)-oriented La _{0.7} Sr _{0.3} MnO ₃ film directly on flexible mica substrate. Journal Physics D: Applied Physics, 2022, 55, 224002.	1.3	6
248	High \$I_{m c}\$ in YBCO Films Grown at Very High Rates by Liquid Mediated Growth. IEEE Transactions on Applied Superconductivity, 2009, 19, 3180-3183.	1.1	5
249	Direct observation of twin deformation in YBa2Cu3O7â^' <i>x</i> thin films by <i>in situ</i> nanoindentation in TEM. Journal of Applied Physics, 2011, 109, .	1.1	5
250	Controllable conduction and hidden phase transitions revealed via vertical strain. Applied Physics Letters, 2019, 114, 252901.	1.5	5
251	Pinning Efficiency of One-Dimensional Artificial Pinning Centers in YBa ₂ Cu ₃ O _{7-x} Thin Films. IEEE Transactions on Applied Superconductivity, 2019, 29, 1-5.	1.1	5
252	Electrochemical removal of anodic aluminium oxide templates for the production of phase-pure cuprous oxide nanorods for antimicrobial surfaces. Electrochemistry Communications, 2020, 120, 106833.	2.3	5

#	Article	IF	CITATIONS
253	Strain Effects on the Growth of La _{0.7} Sr _{0.3} MnO ₃ (LSMO)–NiO Nanocomposite Thin Films via Substrate Control. ACS Omega, 2020, 5, 23793-23798.	1.6	5
254	Ultrafast, dry microwave superheating for the synthesis of an SbOx–GNP hybrid anode to investigate the Na-ion storage compatibility in ester and ether electrolytes. Chemical Communications, 2020, 56, 9663-9666.	2.2	5
255	Thermal stability of self-assembled ordered three-phase Au–BaTiO ₃ –ZnO nanocomposite thin films <i>via in situ</i> heating in TEM. Nanoscale, 2020, 12, 23673-23681.	2.8	5
256	Effective doping control in Sm-doped BiFeO ₃ thin films <i>via</i> deposition temperature. RSC Advances, 2020, 10, 40229-40233.	1.7	5
257	Dynamic tuning of dielectric permittivity in BaTiO ₃ via electrical biasing. Materials Research Letters, 2020, 8, 321-327.	4.1	5
258	Overcoming the Anisotropic Growth Limitations of Free‣tanding Singleâ€Crystal Halide Perovskite Films. Angewandte Chemie, 2021, 133, 2661-2668.	1.6	5
259	Tailorable multifunctionalities in ultrathin 2D Bi-based layered supercell structures. Nanoscale, 2021, 13, 16672-16679.	2.8	5
260	Thermal Stability of Nanocrystalline Gradient Inconel 718 Alloy. Crystals, 2021, 11, 53.	1.0	5
261	Epitaxial nanotwinned metals and alloys: synthesis-twin structure–property relations. CrystEngComm, 2021, 23, 6637-6649.	1.3	5
262	Achieving strong and stable nanocrystalline Al alloys through compositional design. Journal of Materials Research, 2022, 37, 183-207.	1.2	5
263	ZnO-AuxCu1â^'x Alloy and ZnO-AuxAl1â^'x Alloy Vertically Aligned Nanocomposites for Low-Loss Plasmonic Metamaterials. Molecules, 2022, 27, 1785.	1.7	5
264	A generalized 3D elastic model for nanoscale, self-assembled oxide-metal thin films with pillar-in-matrix configurations. Acta Materialia, 2022, 228, 117779.	3.8	5
265	Thermally tunable VO2-SiO2 nanocomposite thin-film capacitors. Journal of Applied Physics, 2018, 123, .	1.1	4
266	Integration of Self-Assembled BaZrO ₃ -Co Vertically Aligned Nanocomposites on Mica Substrates toward Flexible Spintronics. Crystal Growth and Design, 2022, 22, 718-725.	1.4	4
267	Self-organization of various "phase-separated―nanostructures in a single chemical vapor deposition. Nano Research, 2020, 13, 1723-1732.	5.8	3
268	Creating Ferromagnetic Insulating La _{0.9} Ba _{0.1} MnO ₃ Thin Films by Tuning Lateral Coherence Length. ACS Applied Materials & Interfaces, 2021, 13, 8863-8870.	4.0	3
269	Recent Advances in Vertically Aligned Nanocomposites with Tunable Optical Anisotropy: Fundamentals and Beyond. Chemosensors, 2021, 9, 145.	1.8	3
270	Thermal Safety Analysis of Disordered Li-Rich Rock salt Li _{1.3} Mn _{0.4} Nb _{0.3} O ₂ Cathode. ACS Applied Energy Materials, 2022, 5, 516-523.	2.5	3

#	Article	IF	CITATIONS
271	Optical dielectric properties of HfO2-based films. Journal of Vacuum Science and Technology A: Vacuum, Surfaces and Films, 2022, 40, .	0.9	3
272	TiN–Fe Vertically Aligned Nanocomposites Integrated on Silicon as a Multifunctional Platform toward Device Applications. Crystals, 2022, 12, 849.	1.0	3
273	Linking far-from-equilibrium defect structures in ceramics to electromagnetic driving forces. Journal of Materials Chemistry A, 2021, 9, 8425-8434.	5.2	2
274	Hybrid Ag–LiNbO3 nanocomposite thin films with tailorable optical properties. Nanoscale Advances, 2021, 3, 1121-1126.	2.2	2
275	Preparative Mass Spectrometry Using a Rotatingâ€Wall Mass Analyzer. Angewandte Chemie, 2020, 132, 7785-7790.	1.6	1
276	Developing nanostructured cathode of thin film SOFC and its characteristics. , 2008, , .		0
277	Nucleation interface of Al-Sb alloys on single crystal Al 2 O 3 substrate. Transactions of Nonferrous Metals Society of China, 2017, 27, 2104-2111.	1.7	0
278	Reducing Leakage Current and Enhancing Polarization in Multiferroic 3D Super-nanocomposites by Microstructure Engineering. Nanotechnology, 2022, , .	1.3	0
279	Interface Engineering for Enhanced Magnetic Vortex Pinning by 1D-BZO APCs in a Wide Angular Range.	0.3	Ο